Draft version March 4, 2023
Typeset using LaTeX **twocolumn** style in AASTeX631

Cosmic Cousins: Identification of a Subpopulation of Binary Black Holes Formed Through Isolated Binary Evolution

Jaxen Godfrey,[1] Bruce Edelman,[1] and Ben Farr[1]

[1] *Institute for Fundamental Science, Department of Physics, University of Oregon, Eugene, OR 97403, USA*

ABSTRACT

Observations of gravitational waves (GWs) from merging compact binaries have become a regular occurrence. The continued advancement of the LIGO-Virgo-KAGRA (LVK) Collaboration detectors have now produced a catalog of over 90 such mergers, from which we can begin to uncover the formation history of merging compact binaries. In this work, we search for subpopulations in the LVK's third gravitational wave transient catalog (GWTC-3) by incorporating discrete latent variables in the hierarchical Bayesian inference framework to probabilistically assign each BBH observation into separate categories associated with distinctly different population distributions. By incorporating formation channel knowledge within the mass and spin correlations found in each category, we find an over density of mergers with a primary mass of $\sim 10 M_\odot$, confidently associated with isolated binary formation. This low-mass subpopulation has a spin magnitude distribution peaking at $a_{\rm peak} = 0.16^{+0.19}_{-0.16}$, exhibits spins preferentially aligned with the binary's orbital angular momentum, is constrained by $15^{+0.0}_{-1.0}$ of our observations, and contributes $82\%^{+8.0\%}_{-16\%}$ to the overall population of BBHs. While we cannot confidently identify the formation history of every event in the catalog, this work is a first step in gaining a deeper understanding of compact binary formation and evolution, and will provide more robust conclusions as the catalog of observations becomes larger.

1. INTRODUCTION

The first detection of gravitational waves (GWs) from a binary black hole (BBH) merger was made by the LIGO-Virgo-KAGRA (LVK) Collaboration on September 14, 2015. Since that fateful day, the LVK has detected nearly 100 compact binary coalescences (CBCs), bringing the third gravitational wave transient catalog (GWTC-3) up to 90 such events. (LIGO Scientific Collaboration et al. 2015; Acernese et al. 2015; Akutsu et al. 2021; Abbott et al. 2016, 2019a, 2021a; The LIGO Scientific Collaboration et al. 2021a). With the maturation of GW Astronomy, novel studies of the universe are possible; we are now able to probe the entire population of merging compact objects in the universe with much greater fidelity than with the sparse, early LVK catalogs (Abbott et al. 2019b, 2021b; The LIGO Scientific Collaboration et al. 2021b). By breaking down the full CBC population into subpopulations based on different source properties- and paired with our theoretical knowledge of stellar astrophysics- we can begin to uncover the formation and evolution of compact binaries (Zevin et al. 2017). The two most common expected formation channels of merging compact objects are isolated formation and dynamical assembly, each predicted to produce binary populations with unique mass and spin characteristics (Farr et al. 2017, 2018; Arca Sedda et al. 2020). The uncertainty in modeled merger rates of each formation channel is large, and the predictions continue to evolve with better understanding of the underlying physics (see Mandel & Broekgaarden (2022) for a thorough review on both modeled and observed merger rates of compact objects). By looking deeper at the correlations between the source properties at a population level, we can begin to look for subpopulations of observations that we can confidently associate with a specific formation channel.

Isolated formation of compact binaries occurs in galactic fields, where two gravitationally bound stars isolated from their environment undergo standard main sequence evolution, each eventually forming into a compact object. Energy loss from GW radiation causes the binary to inspiral, which can eventually lead to merger; however, in order for the binary to merge within a Hubble time, the initial orbital separation of the compact objects must be small (Bavera et al. 2020; Mandel & Broekgaarden 2022). Some process during stellar evolution is

jaxeng@uoregon.edu

therefore required to rapidly decrease the orbital separation down to this limit for systems with much larger initial separations. One proposed mechanism is the "common envelope phase", in which a cloud of non-rotating gas engulfs the two objects (typically after one star has already collapsed into a compact object) and drag forces quickly dissipate orbital energy, thus reducing the orbital separation enough so that the resulting compact binary can merge due to GW emission alone (Belczynski et al. 2016). In dynamical formation scenarios, scattering or exchange interactions between astrophysical bodies in a dense stellar environment are thought to produce binaries capable of merging within a Hubble time (Rodriguez et al. 2016a). There are many theorized models for the main physical processes that contribute to isolated and dynamical formation, but there are few robust and direct predictions of observable quantities from these models. Instead, current predictions of merger rates and population distributions are estimated from numerical simulations, which have large uncertainties due to uncertain underlying physics or poorly constrained initial conditions (Mandel & Broekgaarden 2022; Bavera et al. 2020; Giacobbo & Mapelli 2018; Dominik et al. 2013).

The spin distribution of merging binaries is thought to provide the most direct evidence of their formation channel (Farr et al. 2017, 2018). Isolated binary evolution scenarios predict component spins to be near zero and preferentially aligned with the orbital angular momentum of the binary, though there are processes, such as angular momentum transport and supernova kicks, that can impart a small non-zero and modestly misaligned spin to one or both of the binary objects (Zevin & Bavera 2022; Belczynski et al. 2020; Bavera et al. 2020, 2021). On the other hand, systems assembled dynamically in stellar clusters are thought to have no preferential alignment, producing an isotropically distributed spin tilt distribution (Rodriguez et al. 2016b, 2019). With current data it is difficult to distinguish between these two channels, though studies have at least shown that GWTC-3 is not consistent with entirely dynamical or entirely isolated formation (The LIGO Scientific Collaboration et al. 2021b; Callister et al. 2022; Tong et al. 2022; Edelman et al. 2022b; Fishbach et al. 2022; **?**). Recent studies have found support for a significant contribution of systems formed through dynamical assembly in the population of BBHs inferred from the GWTC-2 and GWTC-3 catalogs (Abbott et al. 2021b; Roulet et al. 2021; The LIGO Scientific Collaboration et al. 2021b; Callister et al. 2022; Galaudage et al. 2021; Tong et al. 2022; Vitale et al. 2022a; Edelman et al. 2022b), though with large uncertainties.

While spin may be the characteristic most directly linked to compact binary formation history, the LVK parameter estimation of individual event spin properties contains large uncertainties, making it difficult to disentangle competing formation channels with spin alone. However, the component masses of individual events are typically inferred with greater certainty than their spin, and there are even features in the mass distribution that may signal the existence of different subpopulations (Tiwari & Fairhurst 2021; Edelman et al. 2022a; The LIGO Scientific Collaboration et al. 2021b; Tiwari 2022; Edelman et al. 2022b). Unfortunately, it can also be challenging to distinguish between the isolated and dynamical formation channels using only component mass, as the models in both scenarios predict masses that significantly overlap (Rodriguez et al. 2016c). Instead, a search for correlated population properties across mass, spin, and redshift may prove to be much more fruitful in distinguishing between the different CBC formation channels (Fishbach et al. 2021; Callister et al. 2021; van Son et al. 2022; Biscoveanu et al. 2022).

Given the evidence for features, i.e. peaks, in the primary mass spectrum (see Figure 1 and The LIGO Scientific Collaboration et al. (2021c); Tiwari (2022); Fishbach & Holz (2017); Talbot & Thrane (2018); Abbott et al. (2019c, 2021b)), in this letter we attempt to identify a component of the BBH primary mass spectrum with spin properties distinct from the rest of the GWTC-3 BBH population, in hopes of identifying a subpopulation of BBHs with mass and spin characteristics indicative of a specific formation channel. We do this by modeling a portion of the BBH primary mass spectrum as a Log-Gaussian peak and allowing the spin distributions of the events categorized in this peak to differ from the rest of the population. As we will detail below, we identified such a component of the mass spectrum and then conducted a follow-up search for events with different primary mass values but similar spin properties to these events.

To search for these different components of the BBH population, we incorporate discrete latent variables in the hierarchical Bayesian inference framework to probabilistically assign events to categories with unique mass and spin distributions. Incorporating these discrete variables during inference allows us to easily infer each BBH's association with each category, in addition to the posterior distributions for astrophysical branching ratios (also referred to as mixing fractions).

The remaining sections of this letter are structured as follows: Section 2 describes the statistical framework with the inclusion of discrete latent variables and the different component models studied. Section 3 presents

the results of our study, including the inferred branching ratios and the inferred subpopulation membership probabilities for each BBH in GWTC-3. In section 4 we discuss the implications of our findings and how it relates to the current understanding of compact binary formation and population synthesis. We finish in section 5, with a summary of the letter and prospects for distinguishing subpopulations in future catalogs after the LVK's fourth observing run.

2. METHODS

2.1. *Statistical Framework*

We employ the typical hierarchical Bayesian inference framework to infer the properties of the population of merging compact binaries given a catalog of observations. The rate of compact binary mergers is modeled as an inhomogeneous Poisson point process (Mandel et al. 2019), with the merger rate per comoving volume V_c (Hogg 1999), source-frame time $T_{\rm src}$ and binary parameters θ defined as:

$$\frac{dN}{dV_c dt_{\rm src} d\theta} = \frac{dN}{dV_c dt_{\rm src}} p(\theta|\Lambda) = \mathcal{R} p(\theta|\Lambda) \tag{1}$$

with $p(\theta|\Lambda)$ the population model, $\mathcal{R}$ the merger rate, and Λ the set of population hyperparameters. Following other population studies (Mandel et al. 2019; Vitale et al. 2022b; Abbott et al. 2021c; The LIGO Scientific Collaboration et al. 2021c), we use the hierarchical likelihood that incorporates selection effects and marginalizes over the merger rate as:

$$\mathcal{L}(\boldsymbol{d}|\Lambda) \propto \frac{1}{\xi(\Lambda)} \prod_{i=1}^{N_{\rm det}} \int d\theta \mathcal{L}(d_i|\theta) p(\theta|\Lambda) \tag{2}$$

Above, $\boldsymbol{d}$ is the set of data containing $N_{\rm det}$ observed events, $\mathcal{L}(d_i|\theta)$ is the individual event likelihood function for the ith event given parameters θ and $\xi(\Lambda)$ is the fraction of merging binaries we expect to detect, given a population described by Λ. The integral of the individual event likelihoods marginalizes over the uncertainty in each event's binary parameter estimation, and is calculated with Monte Carlo integration and by importance sampling, reweighing each set of posterior samples to the likelihood. The detection fraction is calculated with:

$$\xi(\Lambda) = \int d\theta p_{\rm det}(\theta) p(\theta|\Lambda) \tag{3}$$

with $p_{\rm det}(\theta)$ the probability of detecting a binary merger with parameters θ. We calculate this fraction using simulated compact merger signals that were evaluated with the same search algorithms that produced the catalog of observations. With the signals that were successfully detected, we again use Monte Carlo integration to get the overall detection efficiency, $\xi(\Lambda)$.

To model different subpopulations that could exist in the population, we use discrete latent variables that probabilistically associate each binary merger with different models. To model M subpopulations in a catalog of $N_{\rm det}$ detections, we add a latent variable q_i for each merger that can be M different discrete values between 0 and $M-1$, each associated with a separate model, $p_M(\theta|\Lambda)$, and hyperparameters, Λ_M. Evaluating the model (or hyper-prior) for the $i^{\rm th}$ event with binary parameters, θ_i, given latent variable q_i and hyperparameters Λ_M, we have:

$$p(\theta_i|\Lambda, q_i) = p_{M=q_i+1}(\theta_i|\Lambda_{M=q_i+1}) \tag{4}$$

To construct our probabilistic model, we first sample $p_M \sim \mathcal{D}(M)$, from an M-dimensional Dirichlet distribution of equal weights, representing the astrophysical branching ratios of each subpopulation. Then each of the $N_{\rm det}$ discrete latent variables are sampled from a categorical distribution with each category M having probability, p_M. Within the NumPyro (Bingham et al. 2018; Phan et al. 2019) probabilistic programming language, we use the implementation of the `DiscreteHMCGibbs` (Liu 1996) to sample the discrete latent variables, while using the `NUTS` (Hoffman & Gelman 2011) sampler for continuous variables. While this approach may seem computationally expensive, we find that the conditional distributions over discrete latent variables enable Gibbs sampling with similar costs and speeds to the equivalent approach that marginalizes over each discrete latent variable, q_i. We find the same results with either approach and only slight performance differences that depend on specific model specifications, and thus opt for the approach without marginalization. This method also has the advantage that we get posterior distributions on each event's subpopulation assignment without extra steps.

2.2. *Astrophysical Mixture Models*

Given the recent evidence for a $10M_\odot$, $35M_\odot$, and potentially a $25M_\odot$ peak in the BBH primary mass distribution (The LIGO Scientific Collaboration et al. 2021c; Tiwari 2022; Fishbach & Holz 2017; Talbot & Thrane 2018; Abbott et al. 2019c, 2021b), we chose models similar to the Multi Spin model in Abbott et al. (2021b), which is characterised by a power-law plus a Gaussian peak in primary mass, wherein the spin distributions of the two mass components are allowed to differ from each other. In our case, we replace the power law mass components and parametric spin descriptions with non-parametric Basis-Spline functions, in order to

avoid model dependent biases on the resulting distributions. We also choose to parametrize peaks in the primary mass spectrum in terms of log-mass, rather than linear-mass. In both of our model prescriptions, detailed below, the spin magnitude and tilt distributions of each binary component are assumed to be independently and identically distributed (IID), i.e. we fit the same model distribution to both binary spin components per category. To reduce the number of free parameters and thus computational cost, we fix the power law slope of the merger rate with redshift to $\lambda_z = 2.7$. We make use of the mass and spin basis spline (B-Spline) models from Edelman et al. (2022b). All the models and formalism used in our analysis are available in the GWInferno python library, along with the code and data to reproduce this study in this GitHub repository.

2.2.1. *Base Model*

In this model prescription, we categorize the BBH population into $M = 2$ components, which we will refer to as PEAK A and CONTINUUM B, based on their primary mass distributions (continuum here referring to the non-parametric nature of the B-Spline distributions). The PEAK A component is characterised by a truncated Log-Normal peak in primary mass and B-Spline functions in mass ratio, spin magnitude, and tilt angle. The CONTINUUM B component is characterized by B-Spline functions in all mass and spin parameters. We infer the log mean $\log(\mu_m)$ and standard deviation $\sigma_{\log}(m)$ of the peak, along with the B-Spline coefficients $\mathbf{c}$ for all other parameters. During inference PEAK A is associated with $q_i = 0$ (i.e. $M = 1$) and CONTINUUM B is associated with $q_i = 1$ ($M = 2$).

- PEAK A, $M = 1$ (JG: NUMBER parameters). This category assumes a truncated Log-Normal model in primary mass, a B-spline model in spin magnitude a_j, and a B-spline model in $cos(\theta_{\text{tilt}_i})$. Note that since we assume the spins to be IID, the B-Spline spin parameters, such as $\mathbf{c}_{a,1}$, are the same for each binary component $j = 1$ and $j = 2$

$$p_{m,0}(m_1|\Lambda_{m,0}) = \text{Lognormal}_{\text{T}}(m_1|\mu_m, \sigma_m) \quad (5)$$
$$p_{a,0}(a_j|\Lambda_{a,0}) = B_k(a_j|\mathbf{c}_{a,1}) \quad (6)$$
$$p_{\theta,0}(cos(\theta_j)|\Lambda_{\theta,0}) = B_k(cos(\theta_j)|\mathbf{c}_{\theta,1}) \quad (7)$$

- CONTINUUM B, $M = 2$ (JG: NUMBER parameters). The spin models have the same form as PEAK A, but here primary mass is fit to a B-spline function.

$$\log p_{m,1}(m_1|\Lambda_{m,1}) = B_k(m_1|\mathbf{c}_{m,2}) \quad (8)$$
$$p_{a,1}(a_j|\Lambda_{a,1}) = B_k(a_j|\mathbf{c}_{a,2}) \quad (9)$$
$$p_{\theta,1}(cos(\theta_j)|\Lambda_{\theta,1}) = B_k(cos(\theta_j)|\mathbf{c}_{\theta,2}) \quad (10)$$

2.2.2. *Composite Mass Model*

To investigate whether other parts of the primary mass spectrum may have similar spin characteristics to PEAK A, we construct a composite mass model, wherein we include a new category CONTINUUM A, described by a B-Spline in primary mass but force it to have the same spin distributions as PEAK A. CONTINUUM Bis still included and is described by it's own spin distributions. For this model prescription, we chose to marginalize over the discrete variables q_i during sampling, in order to sample slightly more efficiently.

- PEAK A, $M = 1$ (JG: NUMBER parameters). This category assumes a truncated Log-Normal model in primary mass, a B-spline model in spin magnitude a_i, and a B-spline model in $cos(\theta_{\text{tilt}_i})$.

$$p_m(m_1|\Lambda_m) = \text{Lognormal}_{\text{T}}(m_1|\mu_m, \sigma_m) \quad (11)$$
$$p_a(a_j|\Lambda_a) = B_k(a_j|\mathbf{c}_{a,1}) \quad (12)$$
$$p_\theta(cos(\theta_j)|\Lambda_\theta) = B_k(cos(\theta_j)|\mathbf{c}_{\theta,1}) \quad (13)$$

- CONTINUUM A, $M = 2$ (JG: NUMBER parameters). The spin models are the same as the previous category, but here primary mass is fit to a B-spline function.

$$\log p_m(m_1|\Lambda_m) = B_k(m_1|\mathbf{c}_{m,2}) \quad (14)$$
$$p_a(a_j|\Lambda_a) = B_k(a_j|\mathbf{c}_{a,2}) \quad (15)$$
$$p_\theta(cos(\theta_j)|\Lambda_\theta) = B_k(cos(\theta_j)|\mathbf{c}_{\theta,2}) \quad (16)$$

- CONTINUUM B, $M = 3$ (JG: NUMBER parameters). Here, both primary mass and spin are fit to B-Splines.

$$\log p_m(m_1|\Lambda_m) = B_k(m_1|\mathbf{c}_{m,3}) \quad (17)$$
$$p_a(a_j|\Lambda_a) = B_k(a_j|\mathbf{c}_{a,3}) \quad (18)$$
$$p_\theta(cos(\theta_j)|\Lambda_\theta) = B_k(cos(\theta_j)|\mathbf{c}_{\theta,3}) \quad (19)$$

3. RESULTS

- Start by introducing the dataset (GWTC-3) and threshold/cuts on catalog for our dataset
- Show results of main run model – mass dist – spin dists etc
- Discuss more specific details on different subpopulation mass/spin dists
- Talk about astrophysical branching ratios of subpopulations and which observations were "put" within each of the subpops

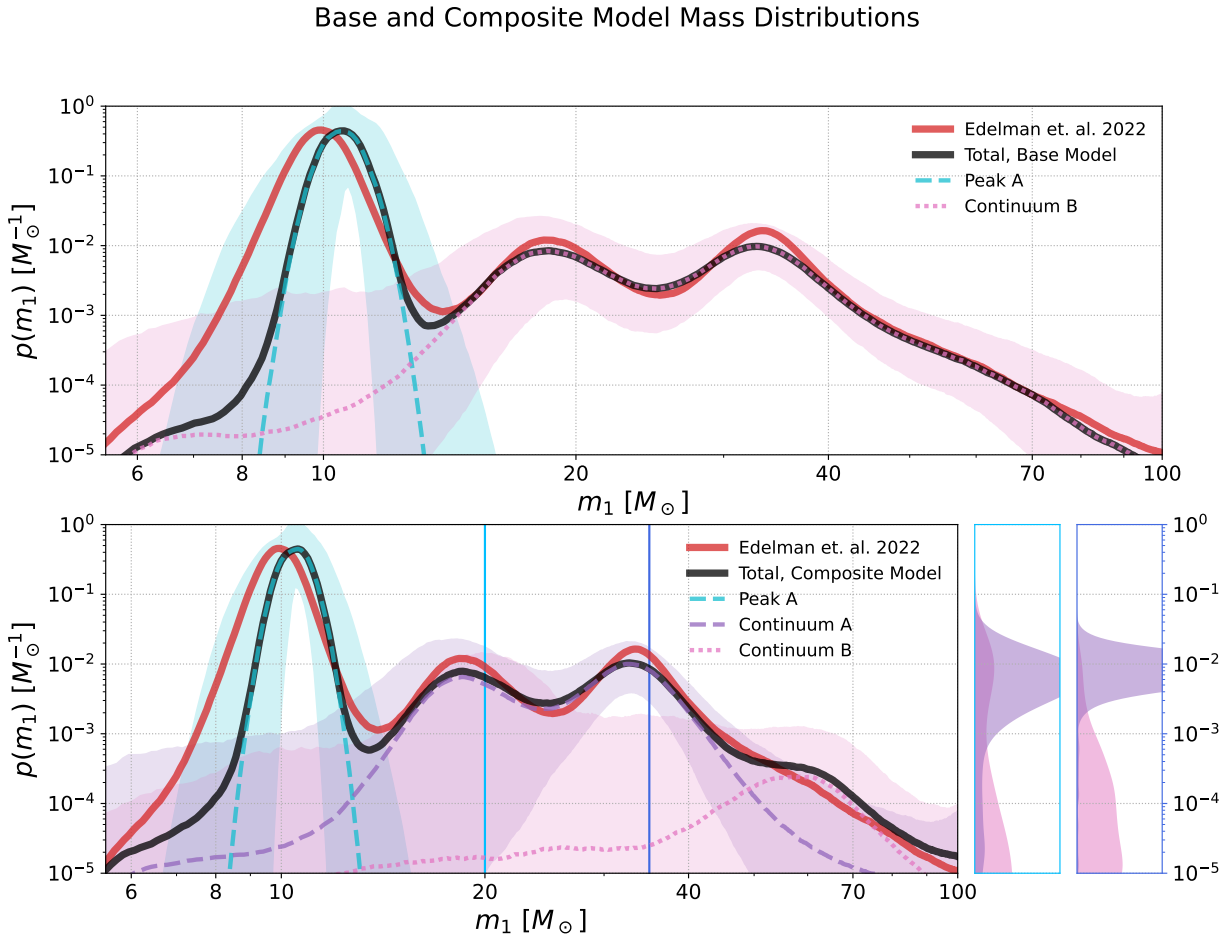

Figure 1. The marginal primary mass distribution

- Quantitative statements on spin mag dist of our isolated subpopulation
- Quantitative statements on spin orientation dist of our isolated subpop. How much does it prefer aligned spins over the other subpops?

With these models and framework in hand, we infer the mass and spin distributions with the recently released LVK catalog of gravitational wave observations, GWTC-3 The LIGO Scientific Collaboration et al. (2021a). We perform the same BBH threshold cuts on the catalog done by the LVK's accompnaying population analysis Abbott et al. (2021c), which leaves us with 70 BBH mergers. Additionally, we choose to remove GW190814 from our anlaysis, as it is likely an outlier of the total BBH population and is not very well understood JG: CITE THIS. With the 69 remaining events, we are able to infer the mass and spin distributions of two potential BBH subpopulations, detailed below.

3.1. *BBH Mass and Spin Distributions*

Figure 1 shows the mass distributions of the BASE MODEL, as well as the the total primary mass distribution inferred by Edelman et al. (2022b) for comparison. As seen in the figure, the total BBH primary mass distribution of the BASE MODEL is statistically consistent with that inferred by Edelman et al. (2022b). Inspecting the components, PEAK A and CONTINUUM B, we see that PEAK A identifies a peak in the primary mass spectrum near $10M_\odot$ while CONTINUUM B describes the rest of the spectrum above the peak. Interestingly, even though the $35M_\odot$ peak was the first observed departure from power law-like behaviour in the mass spectrum, it's spin characteristics are perhaps not as distinct as the $10M_\odot$ peak for PEAK A to isolate it from the rest of the population. As we will discuss later, this does not necessarily imply that the $35M_\odot$ peak does not have spin characteristics distinct from other parts of the mass spectrum. Figure 3 shows the inferred spin magnitude and tilt distributions for the two components. We see that the events categorized in PEAK A prefer lower

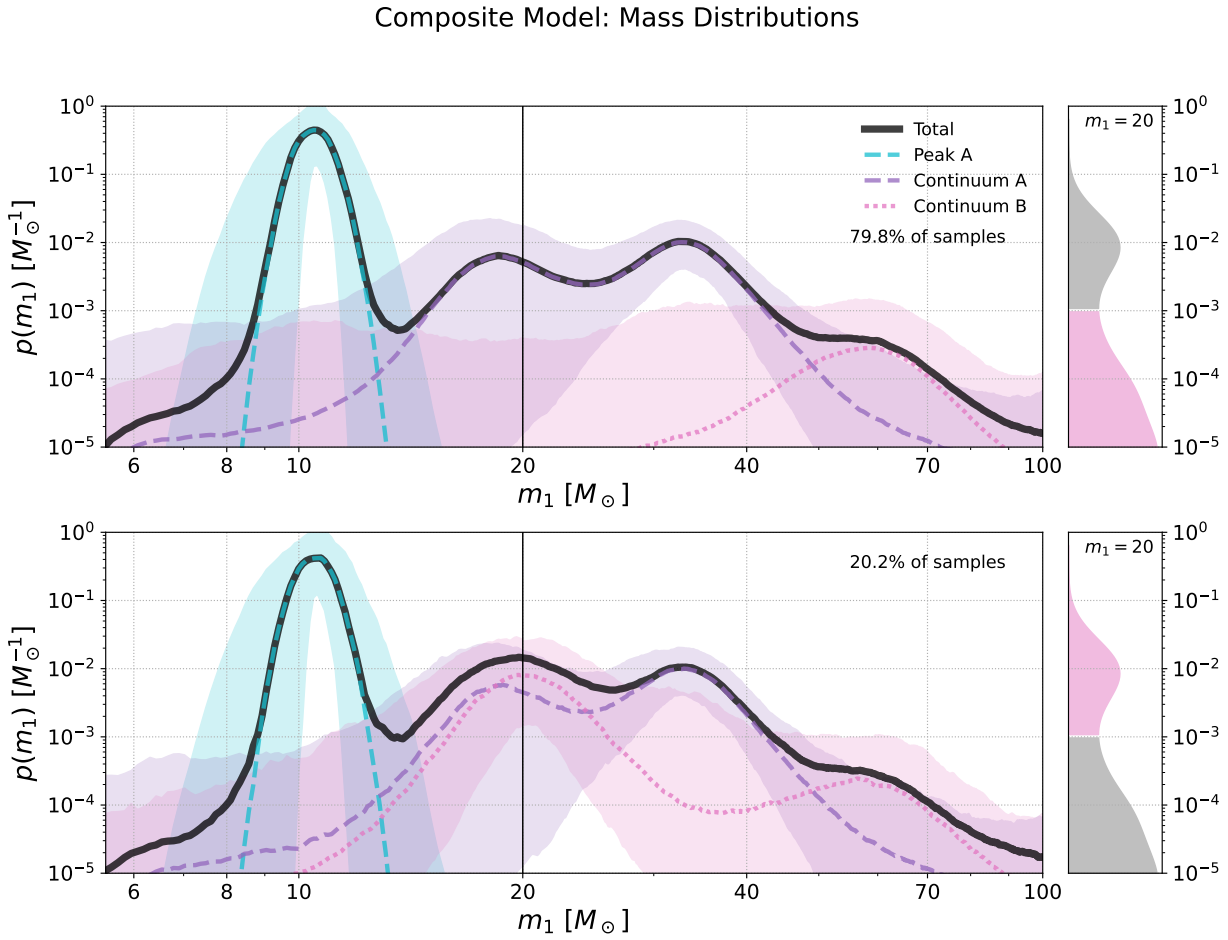

Figure 2. The marginal primary mass distribution

spins than those in CONTINUUM B and have a stronger preference for alignment than their higher mass counterparts. In fact, the tilt distribution of PEAK A peaks at $\cos(\theta_{\rm peak,PA}) = 0.53^{+0.47}_{-1.0}$ while that of CONTINUUM B peaks at $\cos(\theta_{\rm peak,CB}) = 0.17^{+0.83}_{-0.81}$. Given that isolated binary evolution is theorized to produce a population of BBH's with similar mass and spin characteristics JG: CITE, we conclude that PEAK A is consistent with a subpopulation of BBH's formed through isolated binary evolution. Due to the rather large uncertainties in the measured spin parameters, it's important to note that these spin features only hint at preferences of a given subset of events and should be taken with a grain of salt. To confidently associate these BBH's with the field formation channel, more observations are needed. The need for more data is even more apparent when we consider the rest of the BBH population and the results of the COMPOSITE MODEL.

The primary mass distributions of the COMPOSITE MODEL are shown in the bottom panel of Figure 1, again plotted alongside the total distribution inferred by Edelman et al. (2022b). From this figure, we see that the events in the $\sim 15-50 M_\odot$ range are described by CONTINUUM A, which is the component that shares spin properties with PEAK A. The tail end of the mass spectrum is then picked up by CONTINUUM B. Looking to Figure 3, the top right panel shows that the spin magnitude distribution of PEAK A and CONTINUUM A resembles that of PEAK A from the BASE MODEL, while the distribution of CONTINUUM B is completely uninformed. In the bottom right panel, the tilt distribution of PEAK A and CONTINUUM A in the COMPOSITE MODEL also shares similarities with that of PEAK A in the BASE MODEL, and again CONTINUUM B possess an uninformed distribution.

Given these observations, it may be tempting to claim that all these mid-mass events in CONTINUUM A have spin properties consistent with PEAK A and therefore may be the product of the same formation mechanism as PEAK A; however, a closer look at the results shows

there is some uncertainty in how the $25M_\odot$ peak is categorized. If we plot the value of the primary mass probability density for a subset of posterior draws at a given mass, we would expect the result to be relatively Gaussian; however, when we do this for CONTINUUM B at $m_1 = 20M_\odot$, the resulting collection of probability densities is actually bimodal. Making a cut through the posterior draws at the inflection point between the two modes, we recreate Figure 1 in Figure 2 but for these two different areas of parameter space. The top panel of 2 represents JG: some number % of the posterior draws while the bottom represents JG: some number %. We see that while most of the time, the events near $20M_\odot$ are categorized with CONTINUUM A and therefore associated with the $10M_\odot$ peak and $35M_\odot$ peak, there is a small probability that they are actually associated with the highest mass events and therefore could be consistent with an isotropic spin distribution. Importantly, CONTINUUM A rarely picks up the high mass tail of the mass spectrum, which adds merit to the possibility that the $10M_\odot$ and $35M_\odot$ peaks prefer moderately aligned spins over isotropic ones.

4. ASTROPHYSICAL INTERPRETATION

- What can this new identified subpop help to enlighten in stellar pop synth community?
- can we use spin tilt dist to make statements on supernovae kicks in isolated formation?
- How does this compare to LVK work and other recent work? Are our results consistent or in conflict with dyn/iso fractions?
- report fdyn / fhm and etc

5. CONCLUSION

- Reiterate the motivation of the work
- restate the main conclusions leading us to identify this 10 solar mass peak as isolated
- briefly comment on main astro implications from prev section
- Discuss further work on other ways we can use this method to probe formation channels even deeper. (use spin vs mass dist to disentangle the sub pops. i.e. isotropic tilt for dynamical – aligned tilt for isolated)
- Discuss other applications of discrete latent variables (label for BNS/NSBH/BBH, label for 1G/2G/3G etc)

6. ACKNOWLEDGEMENTS

This research has made use of data, software and/or web tools obtained from the Gravitational Wave Open Science Center (https://www.gw-openscience.org/), a service of LIGO Laboratory, the LIGO Scientific Collaboration and the Virgo Collaboration. The authors are grateful for computational resources provided by the LIGO Laboratory and supported by National Science Foundation Grants PHY-0757058 and PHY-0823459. This work benefited from access to the University of Oregon high performance computer, Talapas. This material is based upon work supported in part by the National Science Foundation under Grant PHY-1807046 and work supported by NSF's LIGO Laboratory which is a major facility fully funded by the National Science Foundation.

Software: SHOWYOURWORK (Luger et al. 2021), ASTROPY (Astropy Collaboration et al. 2013, 2018, 2022), NUMPY (Harris et al. 2020), SCIPY (Virtanen et al. 2020), MATPLOTLIB (Hunter 2007), JAX (Bradbury et al. 2018), NUMPYRO (Bingham et al. 2018; Phan et al. 2019),

REFERENCES

Abbott, B. P., Abbott, R., Abbott, T. D., et al. 2016, PhRvL, 116, 061102, doi: 10.1103/PhysRevLett.116.061102

—. 2019a, Physical Review X, 9, 031040, doi: 10.1103/PhysRevX.9.031040

—. 2019b, ApJL, 882, L24, doi: 10.3847/2041-8213/ab3800

—. 2019c, ApJL, 882, L24, doi: 10.3847/2041-8213/ab3800

Abbott, R., Abbott, T. D., Abraham, S., et al. 2021a, Physical Review X, 11, 021053, doi: 10.1103/PhysRevX.11.021053

—. 2021b, ApJL, 913, L7, doi: 10.3847/2041-8213/abe949

—. 2021c, ApJL, 913, L7, doi: 10.3847/2041-8213/abe949

Acernese, F., Agathos, M., Agatsuma, K., et al. 2015, Classical and Quantum Gravity, 32, 024001, doi: 10.1088/0264-9381/32/2/024001

Akutsu, T., Ando, M., Arai, K., et al. 2021, Progress of Theoretical and Experimental Physics, 2021, 05A102, doi: 10.1093/ptep/ptab018

Arca Sedda, M., Mapelli, M., Spera, M., Benacquista, M., & Giacobbo, N. 2020, ApJ, 894, 133, doi: 10.3847/1538-4357/ab88b2

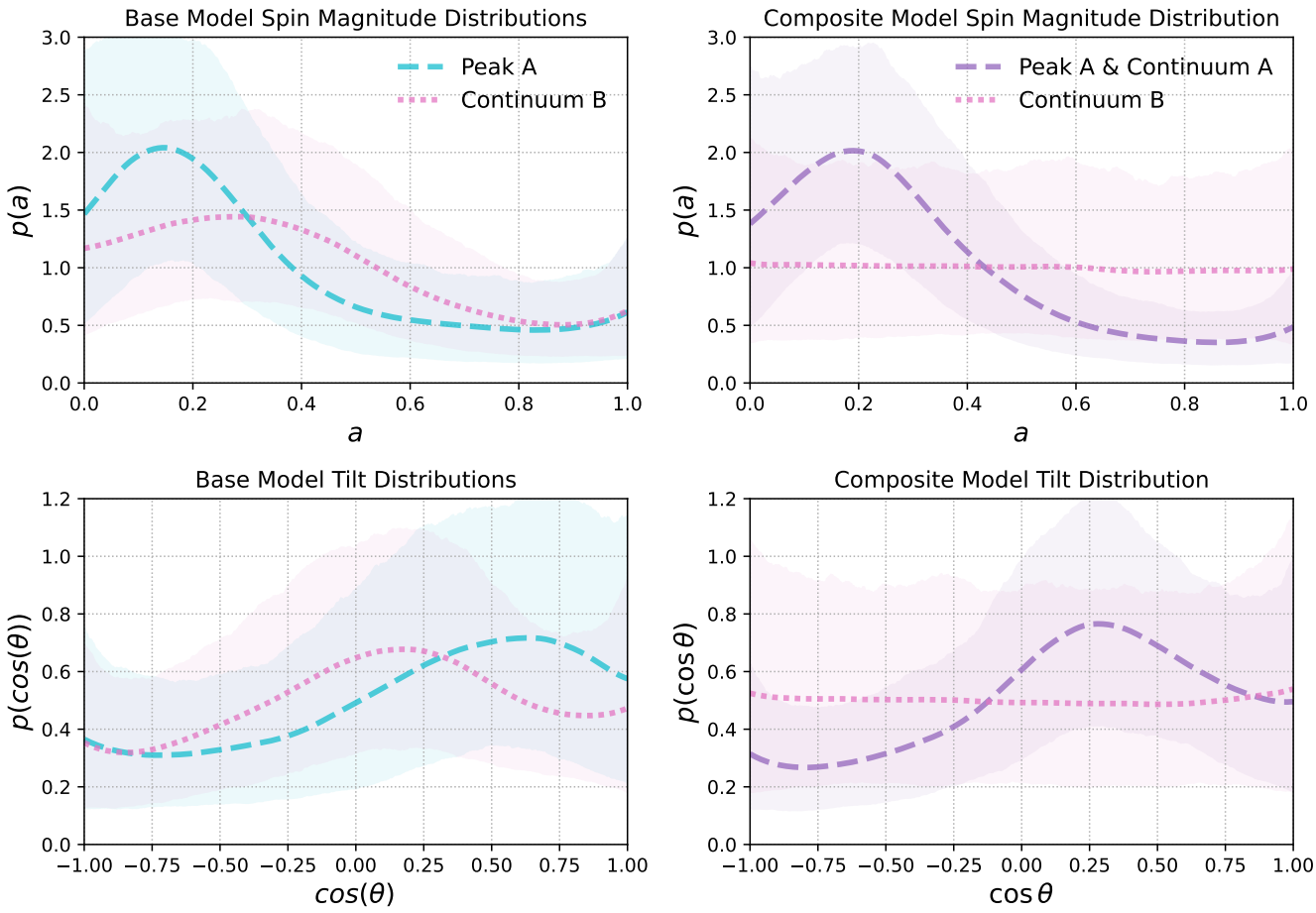

Figure 3. The marginal primary spin magnitude distribution

Astropy Collaboration, Robitaille, T. P., Tollerud, E. J., et al. 2013, A&A, 558, A33, doi: 10.1051/0004-6361/201322068

Astropy Collaboration, Price-Whelan, A. M., Sipőcz, B. M., et al. 2018, AJ, 156, 123, doi: 10.3847/1538-3881/aabc4f

Astropy Collaboration, Price-Whelan, A. M., Lim, P. L., et al. 2022, ApJ, 935, 167, doi: 10.3847/1538-4357/ac7c74

Bavera, S. S., Fragos, T., Qin, Y., et al. 2020, A&A, 635, A97, doi: 10.1051/0004-6361/201936204

Bavera, S. S., Fragos, T., Zevin, M., et al. 2021, A&A, 647, A153, doi: 10.1051/0004-6361/202039804

Belczynski, K., Holz, D. E., Bulik, T., & O'Shaughnessy, R. 2016, Nature, 534, 512, doi: 10.1038/nature18322

Belczynski, K., Klencki, J., Fields, C. E., et al. 2020, A&A, 636, A104, doi: 10.1051/0004-6361/201936528

Bingham, E., Chen, J. P., Jankowiak, M., et al. 2018, arXiv e-prints, arXiv:1810.09538. https://arxiv.org/abs/1810.09538

Biscoveanu, S., Callister, T. A., Haster, C.-J., et al. 2022, ApJL, 932, L19, doi: 10.3847/2041-8213/ac71a8

Bradbury, J., Frostig, R., Hawkins, P., et al. 2018, JAX: composable transformations of Python+NumPy programs, 0.3.13. http://github.com/google/jax

Callister, T. A., Haster, C.-J., Ng, K. K. Y., Vitale, S., & Farr, W. M. 2021, ApJL, 922, L5, doi: 10.3847/2041-8213/ac2ccc

Callister, T. A., Miller, S. J., Chatziioannou, K., & Farr, W. M. 2022, ApJL, 937, L13, doi: 10.3847/2041-8213/ac847e

Dominik, M., Belczynski, K., Fryer, C., et al. 2013, ApJ, 779, 72, doi: 10.1088/0004-637X/779/1/72

Edelman, B., Doctor, Z., Godfrey, J., & Farr, B. 2022a, ApJ, 924, 101, doi: 10.3847/1538-4357/ac3667

Edelman, B., Farr, B., & Doctor, Z. 2022b, arXiv e-prints, arXiv:2210.12834. https://arxiv.org/abs/2210.12834

Farr, B., Holz, D. E., & Farr, W. M. 2018, ApJL, 854, L9, doi: 10.3847/2041-8213/aaaa64

Farr, W. M., Stevenson, S., Miller, M. C., et al. 2017, Nature, 548, 426, doi: 10.1038/nature23453

Fishbach, M., & Holz, D. E. 2017, ApJL, 851, L25, doi: 10.3847/2041-8213/aa9bf6

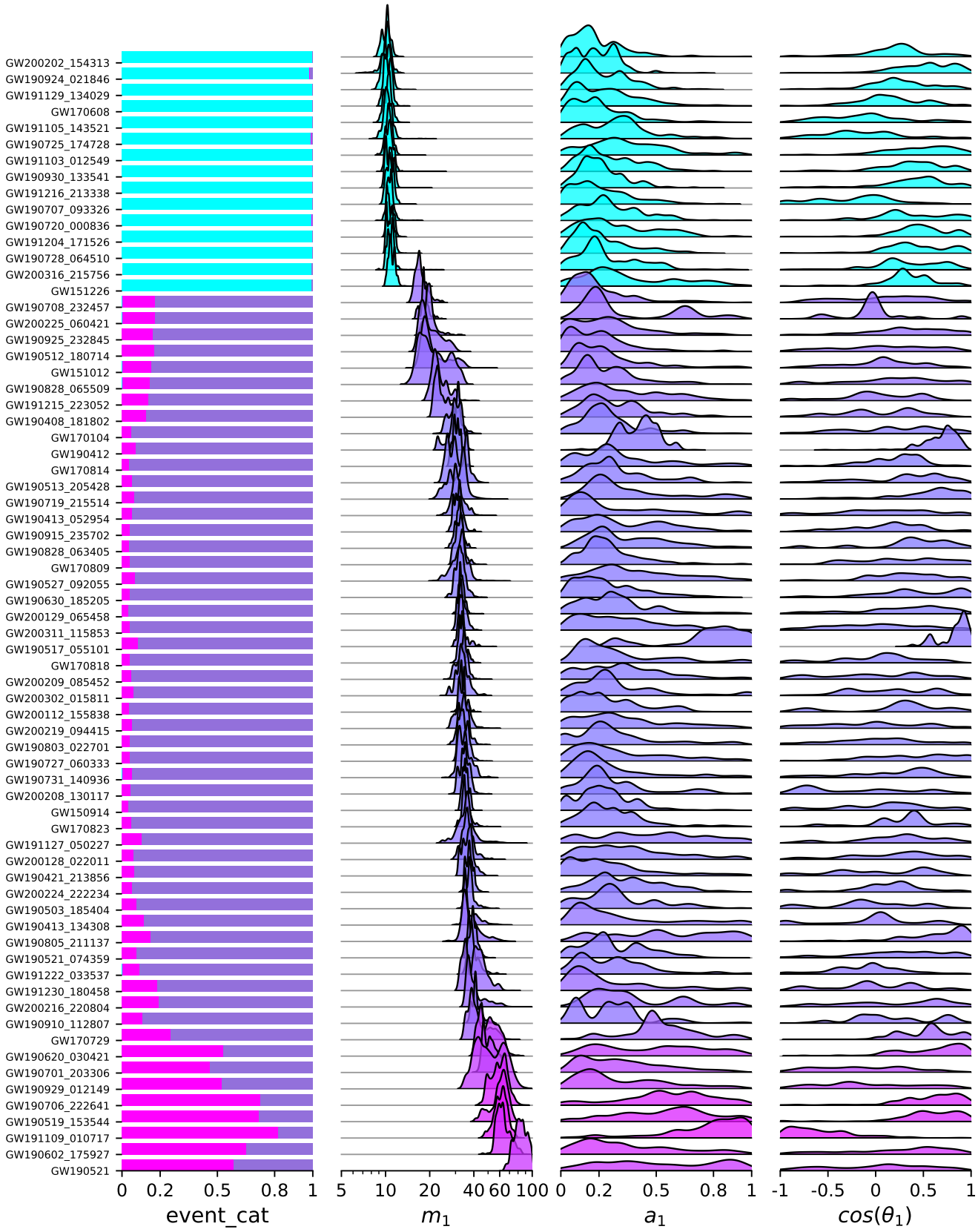

Figure 4. ridgeplot

Fishbach, M., Kimball, C., & Kalogera, V. 2022, ApJL, 935, L26, doi: 10.3847/2041-8213/ac86c4

Fishbach, M., Doctor, Z., Callister, T., et al. 2021, ApJ, 912, 98, doi: 10.3847/1538-4357/abee11

Galaudage, S., Talbot, C., Nagar, T., et al. 2021, ApJL, 921, L15, doi: 10.3847/2041-8213/ac2f3c

Giacobbo, N., & Mapelli, M. 2018, MNRAS, 480, 2011, doi: 10.1093/mnras/sty1999

Harris, C. R., Millman, K. J., van der Walt, S. J., et al. 2020, Nature, 585, 357, doi: 10.1038/s41586-020-2649-2

Hoffman, M. D., & Gelman, A. 2011, arXiv e-prints, arXiv:1111.4246. https://arxiv.org/abs/1111.4246

Hogg, D. W. 1999, arXiv e-prints, astro. https://arxiv.org/abs/astro-ph/9905116

Hunter, J. D. 2007, Computing in Science and Engineering, 9, 90, doi: 10.1109/MCSE.2007.55

LIGO Scientific Collaboration, Aasi, J., Abbott, B. P., et al. 2015, Classical and Quantum Gravity, 32, 074001, doi: 10.1088/0264-9381/32/7/074001

Liu, J. S. 1996, Biometrika, 83, 681

Luger, R., Bedell, M., Foreman-Mackey, D., et al. 2021, arXiv e-prints, arXiv:2110.06271. https://arxiv.org/abs/2110.06271

Mandel, I., & Broekgaarden, F. S. 2022, Living Reviews in Relativity, 25, 1, doi: 10.1007/s41114-021-00034-3

Mandel, I., Farr, W. M., & Gair, J. R. 2019, MNRAS, 486, 1086, doi: 10.1093/mnras/stz896

Phan, D., Pradhan, N., & Jankowiak, M. 2019, arXiv e-prints, arXiv:1912.11554. https://arxiv.org/abs/1912.11554

Rodriguez, C. L., Chatterjee, S., & Rasio, F. A. 2016a, PhRvD, 93, 084029, doi: 10.1103/PhysRevD.93.084029

Rodriguez, C. L., Zevin, M., Amaro-Seoane, P., et al. 2019, PhRvD, 100, 043027, doi: 10.1103/PhysRevD.100.043027

Rodriguez, C. L., Zevin, M., Pankow, C., Kalogera, V., & Rasio, F. A. 2016b, ApJL, 832, L2, doi: 10.3847/2041-8205/832/1/L2

—. 2016c, ApJL, 832, L2, doi: 10.3847/2041-8205/832/1/L2

Roulet, J., Chia, H. S., Olsen, S., et al. 2021, PhRvD, 104, 083010, doi: 10.1103/PhysRevD.104.083010

Talbot, C., & Thrane, E. 2018, ApJ, 856, 173, doi: 10.3847/1538-4357/aab34c

The LIGO Scientific Collaboration, the Virgo Collaboration, the KAGRA Collaboration, et al. 2021a, arXiv e-prints, arXiv:2111.03606. https://arxiv.org/abs/2111.03606

—. 2021b, arXiv e-prints, arXiv:2111.03634. https://arxiv.org/abs/2111.03634

—. 2021c, arXiv e-prints, arXiv:2111.03634. https://arxiv.org/abs/2111.03634

Tiwari, V. 2022, ApJ, 928, 155, doi: 10.3847/1538-4357/ac589a

Tiwari, V., & Fairhurst, S. 2021, ApJL, 913, L19, doi: 10.3847/2041-8213/abfbe7

Tong, H., Galaudage, S., & Thrane, E. 2022, arXiv e-prints, arXiv:2209.02206. https://arxiv.org/abs/2209.02206

van Son, L. A. C., de Mink, S. E., Callister, T., et al. 2022, ApJ, 931, 17, doi: 10.3847/1538-4357/ac64a3

Virtanen, P., Gommers, R., Oliphant, T. E., et al. 2020, Nature Methods, 17, 261, doi: 10.1038/s41592-019-0686-2

Vitale, S., Biscoveanu, S., & Talbot, C. 2022a, arXiv e-prints, arXiv:2209.06978. https://arxiv.org/abs/2209.06978

Vitale, S., Gerosa, D., Farr, W. M., & Taylor, S. R. 2022b, in Handbook of Gravitational Wave Astronomy. Edited by C. Bambi, 45, doi: 10.1007/978-981-15-4702-7_45-1

Zevin, M., & Bavera, S. S. 2022, ApJ, 933, 86, doi: 10.3847/1538-4357/ac6f5d

Zevin, M., Pankow, C., Rodriguez, C. L., et al. 2017, ApJ, 846, 82, doi: 10.3847/1538-4357/aa8408